CRYSTAL GROWTH & DESIGN

pubs.acs.org/crystal

Article

Thiocarbamoyl Disulfides as Inhibitors of Urease and Ammonia Monooxygenase: Crystal Engineering for Novel Materials

Lucia Casali,[#] Luca Mazzei,[#] Renren Sun, Michele R. Chierotti, Roberto Gobetto,* Dario Braga, Fabrizia Grepioni,* and Stefano Ciurli*

Cite This: *Cryst. Growth Des.* 2022, 22, 4528−4537

Read Online

ACCESS | Metrics & More | Article Recommendations | Supporting Information

ABSTRACT: The environmental sustainability of soil nitrogen fertilization is essential for the primary production of food for an expanding human population. In this framework, the control of soil enzymatic activities that impact the release of N-based compounds either in the atmosphere or in the underground waters is critical. The two enzymes that act as key players in the biogeochemical cycle of nitrogen are urease and ammonia monooxygenase (AMO), respectively, nickel- and copper-dependent enzymes. This article reveals the high efficacy of three molecules of the thiurams family, namely, thiram (tetramethylthiuram disulfide, TMTD), disulfiram (tetraethylthiuram disulfide, TETD), and tetraisopropylthiuram disulfide (TIPTD) as inhibitors of both the activities of jack bean (*Canavalia ensiformis*) urease (JBU) and *Nitrosomonas europaea* AMO. The water solubility of these compounds was significantly improved by the preparation of three novel inclusion complexes of *β*-cyclodextrin with TMTD, TETD, and TIPTD by mechanochemical synthesis, using green technology. The resulting *β*-CD·thiuram complexes *β*-CD·TMTD, $(\beta\text{-CD})_2$·TETD, and $(\beta\text{-CD})_2$·TIPTD were all characterized by powder X-ray diffraction, thermogravimetric analysis, and solid-state NMR. A conformational polymorph of TIPTD was also detected and isolated via hot stage microscopy, and structurally characterized by single-crystal X-ray diffraction. Biological tests of enzymatic inhibition performed on JBU and AMO with the *β*-CD·thiuram complexes showed the same inhibition efficacy as the isolated molecules, suggesting that the active species is, in all cases, the free thiuram, likely in equilibrium with the adduct in solution. These results have a great potential for improving the nitrogen use efficiency of soil fertilizers for a greener environment.

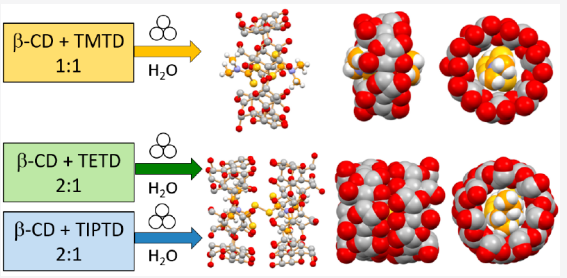

INTRODUCTION

To sustain the food demand by the world population, which will reach 9 billion by the year 2050,[1] a 70−100% expansion in global agricultural production is needed.[2] Nitrogen (N) is a critical nutrient for primary food production by agriculture,[3] and therefore, soil nitrogen fertilization must be carried out to increase crop yield.[4] Around 60% of all nitrogen fertilizers in use are based on urea $[CO(NH_2)_2]$.[5] Upon deposition in soil, urea is rapidly hydrolyzed to ammonium (NH_4^+) and hydrogen carbonate (HCO_3^-), a process catalyzed by the nickel-dependent enzyme urease (urea amidohydrolase, EC 3.5.1.5).[6,7] The active site of urease contains two Ni(II) ions (Figure 1a) that are responsible for making this enzyme the most efficient biological catalyst.[8] The hydrolysis causes a rapid pH increase in the medium that leads to the formation of gaseous ammonia (NH_3) and consequent N loss from soil. The NH_4^+ ion formed upon urea hydrolysis serves as a nutrient to plants as well as for aerobic respiration conducted by ammonia oxidizing bacteria (AOB) such as *Nitrosomonas* (*N.*) *europaea*, which are responsible for the formation of nitrite (NO_2^-), followed by its further oxidation to nitrate (NO_3^-) by nitrite oxidizing bacteria (NOB) living in symbiosis with AOBs.[4,9]

This nitrification process is made of several steps, the first of which, namely, the conversion of NH_4^+ to hydroxylamine (NH_2OH), is catalyzed by ammonia monooxygenase (AMO),[10] a membrane-bound metallo-enzyme containing a Cu(II)/Cu(I) ion in the active site (Figure 1b).[11] The second step of oxidation of NH_2OH to nitrite (NO_2^-) is catalyzed by the multiheme Fe-enzyme hydroxylamine oxidoreductase (HAO), while the final oxidation of nitrite to nitrate in NOB is catalyzed by nitrite oxidoreductase (NOR), containing iron−sulfur centers and a molybdenum cofactor.[12,13] The nitrate formed in these processes can either be taken up by plant roots or enter an anaerobic denitrification route back to nitrite and then to gaseous forms of N such as nitric oxide (NO), nitrous oxide (N_2O), and eventually dinitrogen (N_2),[14,15] while a large portion of nitrate is also leached into groundwater.[4] The

Received: April 14, 2022
Revised: June 7, 2022
Published: June 21, 2022

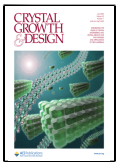

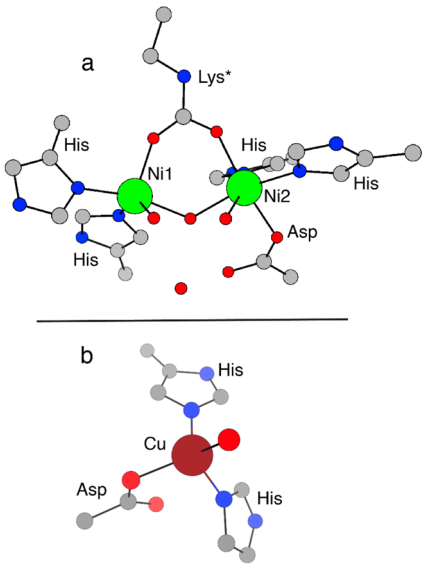

Figure 1. Active sites of urease (a) and ammonia monooxygenase (b). Coloring scheme: C, gray; O, red; N, blue; Ni, green, Cu, brown; water/hydroxide molecules are shown as red spheres.

gaseous species (NH_3, NO, N_2O, N_2) significantly contribute to the greenhouse effect[16] and the formation of air particulate matter,[17] while the leached NO_3^- is a source of eutrophication.[18−20]

Because of these processes, as much as 50% of nitrogen fertilizer applied to soil is not used by crops, a phenomenon that represents a significant economic and environmental cost. These considerations highlight the need to improve N management to make nitrogen fertilization and crop productivity sustainable,[12,13] also through the development of efficient inhibitors of both organic nitrogen mineralization and nitrification.[16,21]

A few nitrification inhibitors are known, among which dicyandiamide (DCD), 2-chloro-6-(trichloromethyl) pyridine (Nitrapyrin, NP), and 3,4-dimethylpyrazole phosphate (DMPP) are the most frequently used in agricultural practice.[4] Even though their mode of action is not known at the molecular level, they are thought to act as chelators of the essential copper atom present in the active site of AMO.[4] Their efficacy to reduce nitrogen losses has been shown to be highly variable,[22,23] while their environmental toxicity, solubility, and concentrations required to modulate nitrification are factors to be considered.[24,25] Therefore, the search for new nitrification inhibitors is required to increase the efficiency of soil nitrogen fertilization toward environmentally sustainable agriculture.

Considering that both AMO and urease possess essential metals in their active sites (Figure 1), an ideal inhibitor could act as a *chelator* for copper or nickel, potentially removing these ions and concomitantly inhibiting both these enzymes. Diethyl-dithiocarbamate, a known strong chelating agent, was reported to inhibit *Paracoccus denitrificans* AMO.[26] The oxidized form of diethyl-dithiocarbamate, originated by the formation of an -S−S- bond, is disulfiram (tetraethylthiuram disulfide, TETD), a drug used to support the treatment of alcohol use disorder[27] and cancer.[28] Disulfiram, together with its methyl derivative thiram (tetramethylthiuram disulfide, TMTD) had also been described as urease inhibitors, but little chemical and biochemical information is available.[29,30] In the present study, the efficiency of thiram, disulfiram, and their tetra-isopropyl derivative (TIPTD) (see Scheme 1) as inhibitors of the nitrification activity of *N. europaea* has been systematically explored. Contextually, the inhibition efficacy of the same compounds on the enzymatic activity of urease from *Canavalia ensiformis* (jack bean urease, JBU) has been investigated with the aim to develop a unique scheme to concurrently modulate the activity of these two key enzymes for soil nitrogen fertilization.

Scheme 1. Representation of the Reagents Used in This Work: the Enzyme Inhibitors Thiram (Tetramethylthiuram Disulfide, TMTD), Disulfiram (Tetraethylthiuram Disulfide, TETD), Tetraisopropylthiuram Disulfide (TIPTD), and *β*-Cyclodextrin (*β*-CD)

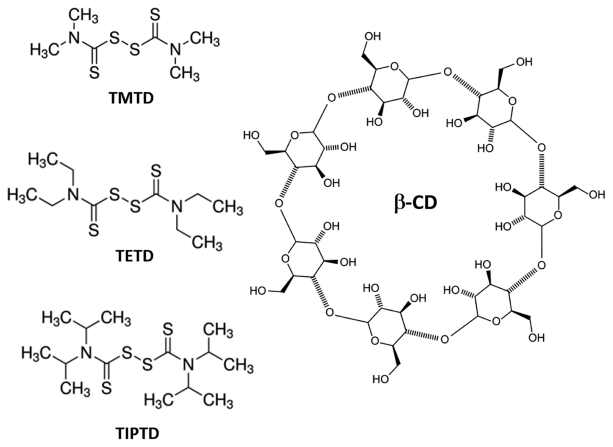

The enzymatic inhibition activity of TMTD, TETD, and TIPTD appeared considerably limited by their poor solubility in water. Following our recent successful attempt to increase the solubility of the nitrification inhibitor NP via encapsulation into hydrated *β*-cyclodextrin (*β*-CD·8H_2O, indicated in the following simply as *β*-CD, Scheme 1),[29] a crystal engineering study[30] was undertaken to develop novel inclusion compounds of these three molecules with *β*-CD, that would feature higher water solubility. The syntheses of inclusion complexes of *β*-CD with TMTD, TETD, and TIPTD were thus performed by mechanochemical reactions of the pure reagents in the presence of a minimum amount of water (see Experimental Section). The resulting materials, characterized by powder X-ray diffraction, thermogravimetry, and solid-state NMR (SSNMR), are all hydrates, with formulas *β*-CD·TMTD·5H_2O, (*β*-CD)$_2$·TETD·14H_2O, and (*β*-CD)$_2$·TIPTD·12H_2O (Scheme 2); for the sake of conciseness, however, throughout this work they will be referred to as *β*-CD·TMTD, (*β*-CD)$_2$·TETD, and (*β*-CD)$_2$·TIPTD, respectively.

The three complexes feature improved solubility in water and act as efficient nitrification and urease inhibitors. These results represent a significant step toward the utilization of novel materials to enhance the efficiency of nitrogen soil fertilization.

EXPERIMENTAL SECTION

Materials. *Canavalia ensiformis* (jack bean) urease (JBU) (Type C-3, powder, ≥600 000 units/g solid) was purchased from Merck Life Science (Milan, Italy) and used without further purification. Stock solutions of JBU (200 U mL^{-1}) were prepared by dissolving the original powder in 50 mM HEPES buffer at pH 7.5 and stored at −80 °C. *Nitrosomonas europaea* cells (*N. europaea*, ATCC 19718) were

https://doi.org/10.1021/acs.cgd.2c00439
Cryst. Growth Des. 2022, 22, 4528−4537

Scheme 2. Syntheses and Stoichiometric Ratios for the Inclusion Compounds Discussed in This Work

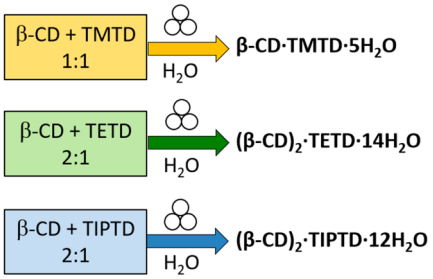

purchased from ATCC (Manassas, VA, USA) and propagated as previously described.[31] Briefly, cells were grown in 1.5 L of ATCC 2265 medium, in the dark at 26 °C. After 72 h, cells were harvested by centrifugation at 10000*g* for 20 min at 4 °C, washed with a 100 mM sodium phosphate buffer at pH 7.5, also containing 2 mM $MgSO_4$ (NaPB buffer), resuspended in 6 mL of the same buffer, and quantified by their total protein content using the biuret assay.[32] Stock aliquots of ca. 0.5 mL with a total protein concentration of ca. 2.5 mg mL^{-1} were prepared and stored at 4 °C.

Tetramethylthiuram disulfide (thiram, TMTD), tetraethylthiuram disulfide (disulfiram, TETD), and tetraisopropylthiuram disulfide (TIPTD) were purchased from Merck Life Science (Milan, Italy). *β*-Cyclodextrin·$8H_2O$ (*β*-CD in the following) was purchased from TCI (Tokyo Chemical Industry Co., Ltd.). Stock solutions used for the enzymatic assays were prepared by dissolving TMTD, TETD, and TIPTD in 100% DMSO, while in the case of their *β*-CD complexes aqueous stock solutions could be prepared, with no addition of DMSO.

Biological Tests of Enzymatic Inhibition. All experiments were conducted at 25 °C in independent triplicates; the measurements were averaged, normalized with respect to a reference experiment performed in the absence of inhibitor, and plotted as a mean percentage ± standard deviation (SD).

Consumption of dioxygen (O_2) by cell cultures of *Nitrosomonas europaea* in the absence and presence of TMTD, TETD, TIPTD, and their complexes with *β*-CD was determined using a Clark-type polarographic electrode (Vernier, Oregon, USA) and a LabQuest2 sensor data collection system (Vernier, Oregon, USA), as previously described.[33] The experiments were initiated by adding one stock aliquot of *N. europaea* cells to NaPB buffer at pH 7.5 containing 10 mM $(NH_4)_2SO_4$ (5 mL final volume) and variable concentrations of the tested compounds (maintaining a DMSO concentration <0.2% in the case of the pure thiurams, which did not significantly affect oxygen consumption by *N. europaea* cells). The traces of recorded O_2 concentration versus time were followed for 20 min and integrated over time to obtain the total amount of O_2 consumed by *N. europaea*. For the integration procedure, the trace describing the O_2 concentration versus time in the absence of substrate was used as baseline. The same setup was used to perform the experiments after a 2-h incubation of *N. europaea* with some of the tested compounds; in these cases, the assays were initiated by adding 10 mM $(NH_4)_2SO_4$ to the incubation mixture.

The inhibition of urease by TMTD, TETD, TIPTD, and their complexes with *β*-CD was investigated by carrying out a spectrophotometric assay in which cresol red was exploited as a colorimetric probe to monitor the overtime change in absorbance at 573 nm due to the increase of pH caused by urease activity, as previously described.[31] Reaction mixtures containing variable concentrations of each compound (1 mL final volume) were prepared in 2 mM HEPES buffer at pH 7.50, 2 mM EDTA, and 30 mg L^{-1} cresol red (CR solution), also containing 10% (v/v) DMSO, and then added with a stock JBU solution at a final concentration of 2 U mL^{-1}. After 1 h of incubation, the experiments were initiated by the addition of an 8 M solution of urea to the mixture (urea final concentration = 100 mM), and the change in absorbance over time at λ = 573 nm was followed over a time interval of 1 min. The activity was calculated by a linear fitting of the straight portion in the absorbance versus time curve.

Mechanochemical Synthesis of *β*-CD Inclusion Complexes. Pure inclusion complexes were obtained by ball milling for 120 min at 20 Hz in an agate jar, using a Retsch Mixer Mill MM 400, the following amounts of reagents: (i) 67.34 mg (0.052 mmol) of *β*-CD and 12.66 mg (0.052 mmol) of TMTD for *β*-CD·TMTD; (ii) 71.68 mg (0.056 mmol) of *β*-CD and 8.32 mg (0.028 mmol) of TETD for $(\beta\text{-CD})_2$·TETD; (iii) 70.30 mg (0.054 mmol) of *β*-CD and 9.70 mg (0.027 mmol) of TIPTD, for $(\beta\text{-CD})_2$·TIPTD, in the presence of 80 *μ*L (0.040 mmol) of water. Reactions between *β*-CD and the three compounds were conducted both in the 1:1 and 2:1 ratio; the final, correct stoichiometry for the three products was determined through a combination of several techniques (see Results and Discussion section).

Powder X-ray Diffraction (PXRD). *Phase identification.* PXRD patterns of *β*-CD·TMTD, $(\beta\text{-CD})_2$·TETD, and $(\beta\text{-CD})_2$·TIPTD and starting materials were collected in Bragg−Brentano geometry on a PANalytical X'Pert Pro Automated diffractometer, equipped with an X'celerator detector, using Cu−K*α* radiation (λ = 1.5418 Å) without a monochromator in the 5−50° 2*θ* range (step size = 0.033°; time/step = 20 s; soller slit = 0.04 rad; antiscatter slit = 1/2; divergence slit = 1/4; 40 mA, 40 kV). *Pawley Refinement.* The PXRD patterns of $(\beta\text{-CD})_2$·TETD and $(\beta\text{-CD})_2$·TIPTD were collected in transmission geometry on a PANalytical X'Pert PRO Automated diffractometer, equipped with a focusing mirror and pixel detector, in the 3−70° 2*θ* range (step size = 0.02608, time/step = 200 s; soller slit = 0.02 rad; 40 kV, 40 mA). Powder diffraction data were analyzed with the software TOPAS4.1.[34] A shifted Chebyshev function with six parameters was used to fit the background.

Single -Crystal X-ray Diffraction. Single-crystal data for the Form II of TIPTD, obtained via HSM (see below), were collected at room temperature with an Oxford XCalibur S CCD diffractometer equipped with a graphite monochromator (Mo−K*α* radiation, λ = 0.71073 Å). The structure was solved by intrinsic phasing with SHELXT5[35] and refined on F^2 by full-matrix least-squares refinement with SHELXL[36] implemented with the Olex2 software. All non-hydrogen atoms were refined anisotropically. The program Mercury[37,38] was used to calculate the powder patterns from single-crystal data and for molecular graphics. See Table S1 for crystal data and details of measurement. Crystal data can be obtained free of charge via www.ccdc.cam.ac.uk/conts/retrieving.html (or from the Cambridge Crystallographic Data Centre, 12 Union Road, Cambridge CB21EZ, UK; fax: (+44)1223-336-033; or e-mail: deposit@ccdc.cam.ac.uk). CCDC 2166004.

Thermogravimetric Analysis (TGA). TGA measurements were performed with a PerkinElmer TGA7 thermogravimetric analyzer, under an N_2 gas flow and at a heating rate of 5.00 °C min^{-1}, in the 30−300 °C and 30−450 °C temperature ranges for TMTD, TETD, and TIPTD and for *β*-CD, *β*-CD·TMTD, $(\beta\text{-CD})_2$·TETD, and $(\beta\text{-CD})_2$·TIPTD, respectively.

DSC. The DSC trace for TIPTD was recorded using a PerkinElmer Diamond differential scanning calorimeter at a heating rate of 5.00 °C min^{-1}. The sample was placed in an open Al pan and analyzed in the 30−150 °C temperature range.

Hot Stage Microscopy (HSM). HSM measurements were carried out on TIPTD Form I, at a heating rate of 10 °C min^{-1}, using a Linkam TMS94 device connected to a Linkam LTS350 platinum plate. Images were taken with a 100× magnification using an optical microscope OLYMPUS BX41 equipped with a NIKON DS FI3 camera. Crystals of Form II suitable for single-crystal X-ray diffraction were obtained upon recrystallization, on cooling, of the melt.

Solid-State NMR Spectroscopy. The ^{13}C CPMAS spectra for all samples *β*-CD·TMTD, $(\beta\text{-CD})_2$·TETD and $(\beta\text{-CD})_2$·TIPTD were acquired with a Jeol ECZR 600 instrument, operating at 600.17 and 150.91 MHz for ^1H and ^{13}C. The powder samples were packed into cylindrical zirconia rotors with a 3.2 mm o.d. and a 60 *μ*L volume. The solid samples were used without further preparations to fill the rotor. ^{13}C CPMAS spectra were acquired at room temperature at a

https://doi.org/10.1021/acs.cgd.2c00439
Cryst. Growth Des. 2022, 22, 4528−4537

spinning speed of 20 kHz, using a ramp cross-polarization pulse sequence with a 90° ^{1}H pulse of 2.0 μs, a contact time of 3.5 ms, and an optimized recycle delay between 1.2 and 36.4 s, with the number of scans ranging between 16 and 63800, depending on the sample. For every spectrum, a two-pulse phase modulation (TPPM) decoupling scheme was used, with a radiofrequency field of 108.5 kHz. The ^{13}C chemical shift scale was calibrated through the methylene signal of external standard glycine, set at 43.7 ppm.

Solubility Tests. The inclusion compounds β-CD·TMTD·5H_2O (12−14 mg), (β-CD)$_2$·TETD·14H_2O (9−10 mg), and (β-CD)$_2$·TIPTD·12H_2O (2−3 mg) were gradually added to three Erlenmeyer flasks containing 50 mL of water, until oversaturation was reached. The suspension was kept under stirring for 24 h to achieve solvent−solute equilibrium. Additional water was then added dropwise into the suspension to dissolve the residual solid. The solubility measurements were repeated three times, as detailed in Table S2.

RESULTS AND DISCUSSION

The impact of increasing concentrations of TMTD, TETD, and TIPTD on the oxidation of NH_4^+ by whole cells of *N. europaea* was investigated. The results indicate that TMTD acts as a potent nitrification inhibitor, with a dose-dependent effect (Figure 2a). Similarly, TETD inhibits nitrification with a dose-dependent effect even though the efficiency is lower than that of TMTD (Figure 2b). On the other hand, TIPTD does not display a dose-dependent effect, and its inhibition potency is lower than TMTD and TETD (Figure 2c). This trend can be ascribed to the increasing steric hindrance of the substituents in these compounds. This effect could be due to either a progressively limiting capability to pass through the outer membrane of this Gram-negative bacterium or to an increased difficulty to access the enzyme active site. To verify this hypothesis, the same assay was carried out for TETD and TIPTD after 2 h of incubation with *N. europaea* cells. In both cases, a much stronger inhibition of O_2 consumption was observed (Figure 2d,e), suggesting an effect due to the cell membrane.

The effects of the three tested compounds on the activity of jack bean (*Canavalia ensiformis*) urease (JBU) were also investigated. The results revealed a strong inhibition of urease by this class of compounds. While TMTD (Figure 3a) and TETD (Figure 3b) have similar inhibition strengths, a lower effect of TIPTD is visible (Figure 3c) and can be again ascribed to the increased steric hindrance of the isopropyl groups, as compared to the methyl and ethyl groups of TMTD and TETD.

The nitrification and urease inhibition assays carried out using the pure TMTD, TETD, and TIPTD, which revealed a significant effect on these compounds on the catalytic activity of these enzymes, also highlighted the scarce solubility in water of all three compounds, prompting us to investigate the possible formation of water-soluble adducts.

Polymorphism in Tetraisopropylthiuram Disulfide (TIPTD). As is customary, we evaluated the stability with temperature of the solids under investigation by differential scanning calorimetry. While TMTD and TETD show a single endothermic peak at 154 and 71 °C, respectively, corresponding to literature values for pure substance melting, a DSC trace on commercial TIPTD shows the presence of an additional endothermic event at ca. 107 °C, followed by melting at 117 °C (see Figure 4 and Figure S7).

To better understand this thermal behavior, we conducted a hot stage microscopy (HSM) measurement (see Figure 5). Crystalline TIPTD Form I was brought to 120 °C at a heating

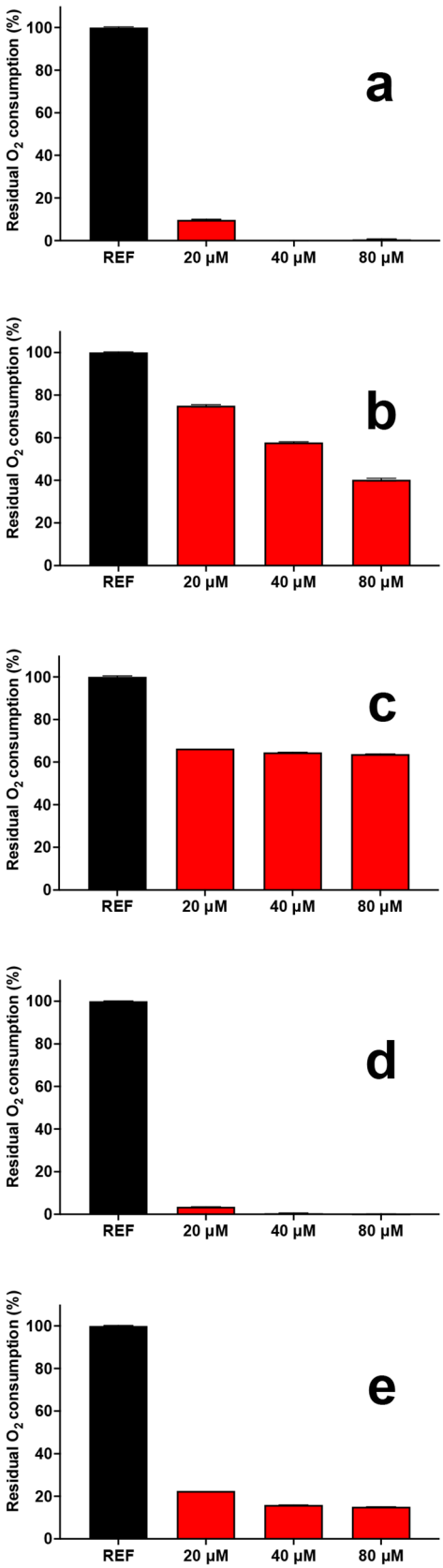

Figure 2. Residual O_2 consumption by *N. europaea* in the presence of increasing concentrations of TMTD (a), TETD (b), and TIPTD (c) at t = 0, and TETD (d) and TIPTD (e) after 2 h incubation.

https://doi.org/10.1021/acs.cgd.2c00439
Cryst. Growth Des. 2022, 22, 4528−4537

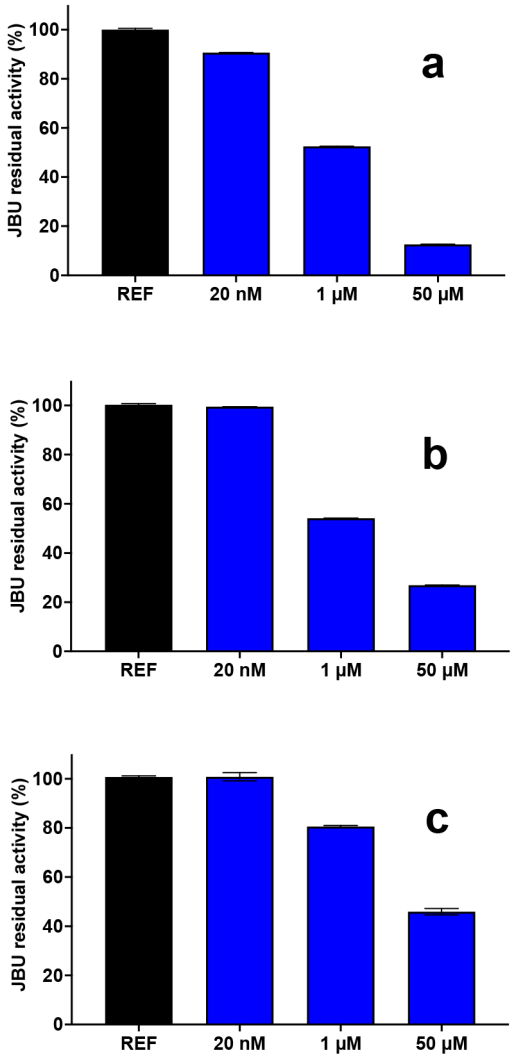

Figure 3. Residual enzymatic activity of JBU in the presence of increasing concentrations of TMTD (a), TETD (b), and TIPTD (c).

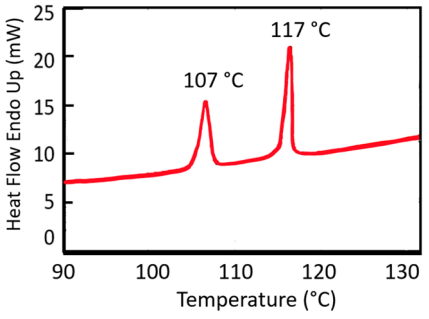

Figure 4. DSC heating cycle for TIPTD Form I (commercial form) heating cycle. Form I transforms into Form II at ca. 107 °C (peak temperature); Form II melts at 117 °C.

rate of 10 °C min^{-1} and observed with an optical microscope in polarized light. In agreement with the DSC measurement, at ca. 110 °C a transformation takes place to a new crystalline phase, that starts melting at 112 °C. The melting process is complete at 120 °C. Upon cooling, recrystallization is observed at ca. 70 °C, i.e., with a large hysteresis.

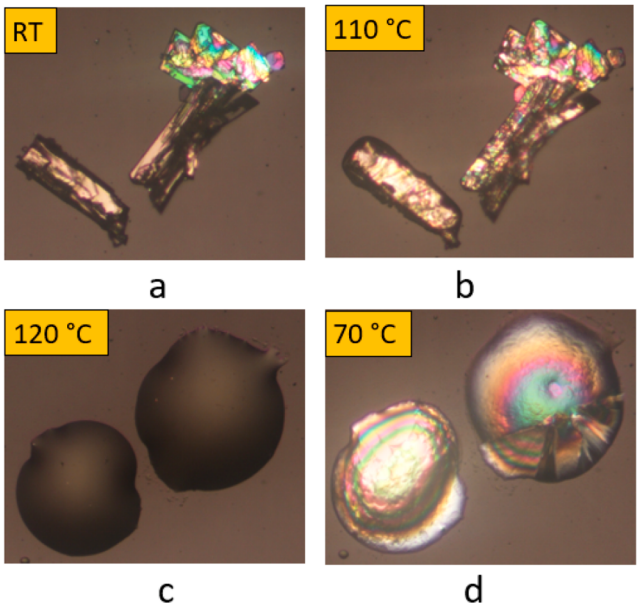

Figure 5. HSM: optical microscope images taken under polarized light on Form I. (a) Room temperature; (b) phase transition to Form II at 110 °C; (c) melting at 120 °C; (d) recrystallization of Form II, on cooling, at 70 °C.

The crystals of the new Form II thus obtained were of sufficiently good quality to allow structural determination via single-crystal X-ray diffraction (see Table S1). As the two polymorphs reversibly interconvert in the solid state, depending on the temperature, they constitute an enantiotropic system. Form II is thus metastable at room temperature and transforms back to Form I in a matter of hours: for this reason, the single-crystal data collection was performed with a short exposure time, to avoid phase transformation during the measurement. TIPTD Form I and Form II are conformational polymorphs, as can be seen from the representation of the molecular structures in the two crystals (Figure 6). Commercial TIPTD, i.e., Form I, corresponds to the form

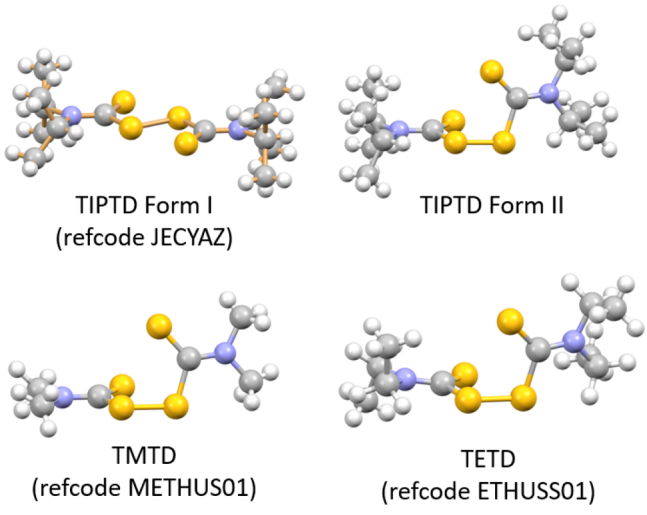

Figure 6. Comparison of the molecular conformation in crystalline TIPTD Form I and II (top) and TMTD and TETD (bottom). The C−S−S−C torsion angle in the four systems is 180°, 87°, 88°, and 91°, respectively.

https://doi.org/10.1021/acs.cgd.2c00439
Cryst. Growth Des. 2022, 22, 4528−4537

deposited in the Cambridge Structural Database (refcode JECYAZ), characterized by a C−S−S−C torsion angle of 180°. A comparison with Form II, TMTD, and TETD (Figure 6) shows that in these three compounds the conformation of the molecular backbone is twisted, with a torsion angle of ca. 88°, 91°, and 87°, respectively. A comparison of the packing efficiency in the four solids shows that the packing coefficient for TIPTD Form II is quite low (only 0.61), while TMTD, TETD, and TIPTD Form I are characterized by packing coefficients of 0.67, 0.68, and 0.66, respectively, which are values commonly observed for molecular solids. Such a large difference is probably the reason for the different conformation of Form I with respect to those observed for the other two thiurams at all temperatures.

Solid-State Synthesis and Structural Characterization of TMTD, TETD, and TIPTD Inclusion Complexes. Cocrystallization attempts of TMTD, TETD, and TIPTD with the goal of improving their solubility in water have been, thus far, unsuccessful. The large hydrophobicity of the thiurams under study, however, suggested an alternative route for the preparation of novel solid-state formulations, namely, their inclusion into β-cyclodextrin (β-CD). A similar approach has been recently reported, in which nitrapyrin, a known inhibitor of ammonia monooxygenase, was shown to form inclusion adducts, with improved water solubility, with β-CD.[29]

The synthesis of all inclusion complexes was performed following a green-chemistry approach, via mechanochemistry.[39] Construction of supramolecular systems and bonds via reaction of crystalline materials in stoichiometric ratios, with the aid of mechanical force, is not only possible, but desirable, fast, often quantitative, and solvent-free. Traces of liquid, however, can be added to facilitate the reaction (water in this case, see Experimental Section). β-Cyclodextrin and the pure thiurams were reacted in both 1:1 and 2:1 stoichiometric ratios; in the case of TMTD, which contains terminal methyl groups, a stoichiometric ratio of 1:1 was invariably observed in the product of the mechanochemical reaction. In the case of TETD and TIPTD, however, the more cumbersome ethyl and isopropyl groups favor a 2:1 stoichiometry ratio, as evidenced by solid-state NMR (see below).

Powder X-ray diffraction measurements on the 1:1 and 2:1 products of the mechanochemical reaction between β-CD and TMTD, TETD, and TIPTD were markedly different from the ones of the pure reagents (see Figures S1, S2, and S3), indicating the formation of new compounds, which were subsequently identified as hydrated β-CD·TMTD, $(\beta\text{-CD})_2$·TETD, and $(\beta\text{-CD})_2$·TIPTD. No single crystals could be grown from solution, and we had to rely on powder data to assign a tentative stoichiometry and packing arrangement.

According to the principle of isostructurality,[40] β-CD molecules generally crystallize in eight possible isostructural series, each of them characterized by similar cell parameters, and therefore by similar powder X-ray diffraction patterns, regardless of the chemical nature of the guest molecules. We recently employed this method for the characterization of β-CD inclusion compounds.[29,41] A Pawley refinement on the experimental pattern of $(\beta\text{-CD})_2$·TETD provided a good match with the isostructural series corresponding to the channel-type crystal structure of β-CD dimers in the triclinic space group *P*1 (see Figure 7a−c and Figure S4); in the case of β-CD·TMTD and $(\beta\text{-CD})_2$·TIPTD, however, no isostructural series could be identified with certainty. We then turned to solid-state NMR spectroscopy (SSNMR, see below) to assess the stoichiometry of the TMTD and TIPTD complexes and compare their behavior with that of the TETD complex.

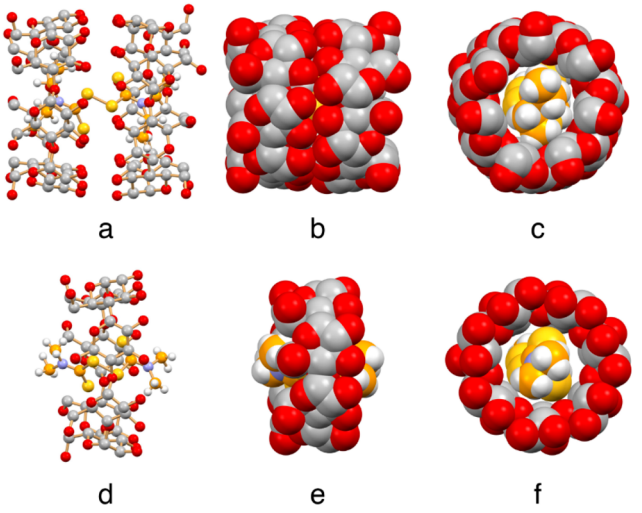

Figure 7. Simulated arrangement along the *b*-axis (a, b) and the *c*-axis (c) of the TETD molecule within the hydrophobic cavity of two β-CD molecules in triclinic *P*1, as inferred from cell parameters (powder data; see Supporting Information) and isostructural series analysis.[40] An analogous simulation for the TMTD inclusion complex is shown in panels d−f. Note how the thiuram is completely embedded within two β-CD molecules in the 2:1 complex $(\beta\text{-CD})_2$·TETD (a−c), while it is protruding out of the β-CD molecule in the 1:1 complex β-CD·TMTD (d−f). Graphical representations obtained with the program Mercury,[37,38] by manual insertion of the thiuram molecules into β-CD. For a simulation of the β-CD molecules arrangement in (a−c), coordinates were taken from the CSD refcode SOBHUM,[42] which also crystallizes with a 2:1 stoichiometry in the isostructural *P*1 triclinic cell.

Solid-State NMR (SSNMR). SSNMR experiments performed on the pure reagents and their β-CD inclusion complexes provide details of the effective formation of the inclusion complexes and their stoichiometry: indeed, for the three systems, all signals appear much broader than for the pure reagents (see Figures 8, 9, 10). This is a well-known behavior[43,44] and can be due to a more dynamic nature of the

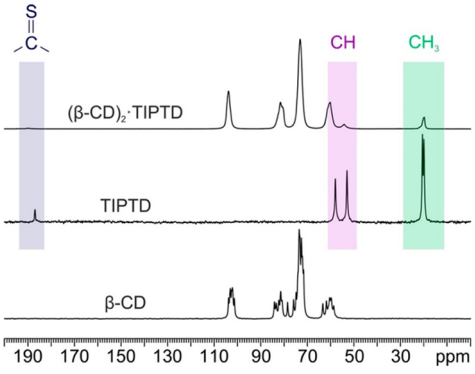

Figure 8. ^{13}C (150.91 MHz) CPMAS spectra of β-CD, TIPTD, and $(\beta\text{-CD})_2$·TIPTD, acquired at room temperature at a spinning speed of 20 kHz. Colored boxes and writings highlight the signals ascribable to the functional groups of TIPTD.

https://doi.org/10.1021/acs.cgd.2c00439
Cryst. Growth Des. 2022, 22, 4528−4537

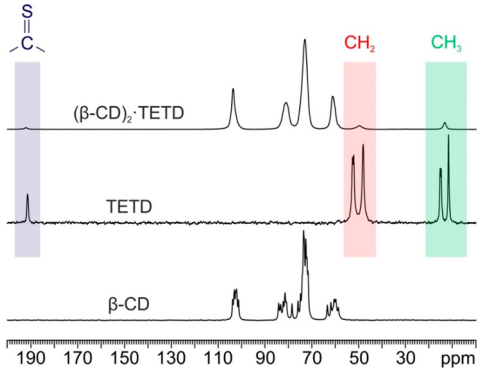

Figure 9. ^{13}C (150.91 MHz) CPMAS spectra of β-CD, TETD, and (β-CD)$_2$·TETD, acquired at room temperature at a spinning speed of 20 kHz. Colored boxes and writings highlight the signals ascribable to the functional groups of TETD. Because of the quantification CPMAS limits, the 2:1 stoichiometry was deducted from the spectra only by combining the information coming from the reagent ratio used during the synthesis and the PXRD data (see main text).

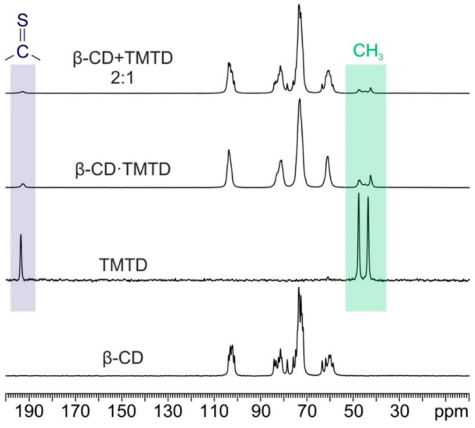

Figure 10. ^{13}C (150.91 MHz) CPMAS spectra of β-CD, TMTD, β-CD·TMTD (1:1), and β-CD + TMTD in a 2:1 ratio, acquired at room temperature at a spinning speed of 20 kHz. Colored boxes and writings highlight the signals ascribable to the functional groups of TMTD.

complex or to a stochastic dispersion of the molecules of thiuram in the complex which increases disorder.

The formation of a 2:1 β-CD−TIPTD inclusion complex was confirmed by comparing its ^{13}C CPMAS spectrum (see Figure 8) with that of (β-CD)$_2$·TETD (see Figure 9) for which the 2:1 stoichiometry was assessed with certainty by XRD. In the case of β-CD with TMTD, the ^{13}C CPMAS spectrum of the sample prepared with a 2:1 stoichiometry was characterized by peaks of unreacted β-CD (see Figure 10). On the other hand, the 1:1 sample provides a spectrum without peaks of unreacted β-CD and with a lower β-CD/TMTD signal ratio with respect to the analogous (β-CD)$_2$·TETD (see Figure 8), indicating the formation of β-CD·TMTD.

Figure 11 reports the overlaid ^{13}C CPMAS spectra of TMTD, TETD, and TIPTD and their respective β-CD adducts in the 180−200 ppm chemical shift range, which features the thiocarboxylic carbon atoms signals: the larger line widths of the signals in the spectra of the complexes as compared to the pure materials are evident; moreover, the splitting of the thiocarboxylic signal of TMTD in β-CD·TMTD, together with the higher number of methyl resonances in the complex than in pure TMTD (see Figure 8), indicates an asymmetry in the two specular fragments of the guest molecule. We can infer that only half of the TMTD molecule is included in the β-CD cavity, while the other protrudes out, or, alternatively, by considering the whole molecule inside the CD, the asymmetry arises from the inequivalence of the two sides of the β-CD (see Figure 7d−f). The latter hypothesis seems more reliable and would justify why the 2:1 complex was not obtained with TMTD.

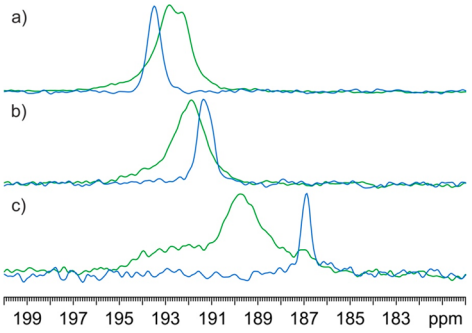

Figure 11. Overlays of the thiocarboxylic regions of the ^{13}C CPMAS spectra of the pure thiurams (in blue) and of the respective complexes with β-CD (in green). (a) TMTD; (b) TETD; (c) TIPTD.

Thermal Behavior of the Inclusion Complexes. Thermogravimetric analysis (TGA) provided further evidence of the formation of the inclusion complexes and was employed to evaluate their water content. TMTD, TETD, and TIPTD traces show that they all degrade in the range 200−250 °C, while β-CD features a weight loss related to dehydration (40−80 °C), followed by degradation at ca. 300 °C (see Figure S5). Upon inclusion into the β-CD cavity, the degradation temperature of thiurams is increased by ca. 50 °C, just below the temperature of β-CD degradation (see Figure S6). In the case of β-CD·TMTD, however, a weight loss ascribable to pure TMTD is detectable before the major one, probably due to its partial inclusion into β-CD in the crystalline edifice, therefore to a more facile removal from β-CD. A weight loss for all compounds in the range 40−100 °C can be attributed to dehydration, with removal of ca. 5, 14, and 12 water molecules, thus allowing the correct formula assignment to the inclusion complexes, i.e., β-CD·TMTD·5H$_2$O, (β-CD)$_2$·TETD·14H$_2$O, and (β-CD)$_2$·TIPTD·12H$_2$O, respectively.

Solubility Tests. Solubility measurements for the three inclusion compounds in water at 20 °C (see Supporting Information), normalized with respect to the thiuram contents, yielded values for the thiuram solubility of 37(2) mg L^{-1} (1.5 × 10^{-4} mol L^{-1}), 18(2) mg L^{-1} (5.9 × 10^{-5} mol L^{-1}), and 6.0(2) mg L^{-1} (1.7 × 10^{-5} mol L^{-1}) for TMTD, TETD, and TIPTD, respectively. Literature solubility values for pure TMTD, TETD, and TIPTD in water at room temperature are 30 mg L^{-1} (1.248 × 10^{-4} mol L^{-1}), 4 mg L^{-1} (1.379 × 10^{-5} mol L^{-1}), and insoluble, respectively.[45] It can be observed, therefore, that the water solubility for all thiurams is significantly enhanced upon complexation with β-CD.

Biological Tests of Enzymatic Inhibition by Inclusion Complexes. The effects of the novel and characterized inclusion complexes β-CD·TMTD, (β-CD)$_2$·TETD, and (β-CD)$_2$·TIPTD obtained by mechanochemical synthesis on the nitrification and urease activity were then investigated. The results indicated that β-CD·TMTD acts as a potent

https://doi.org/10.1021/acs.cgd.2c00439
Cryst. Growth Des. 2022, 22, 4528−4537

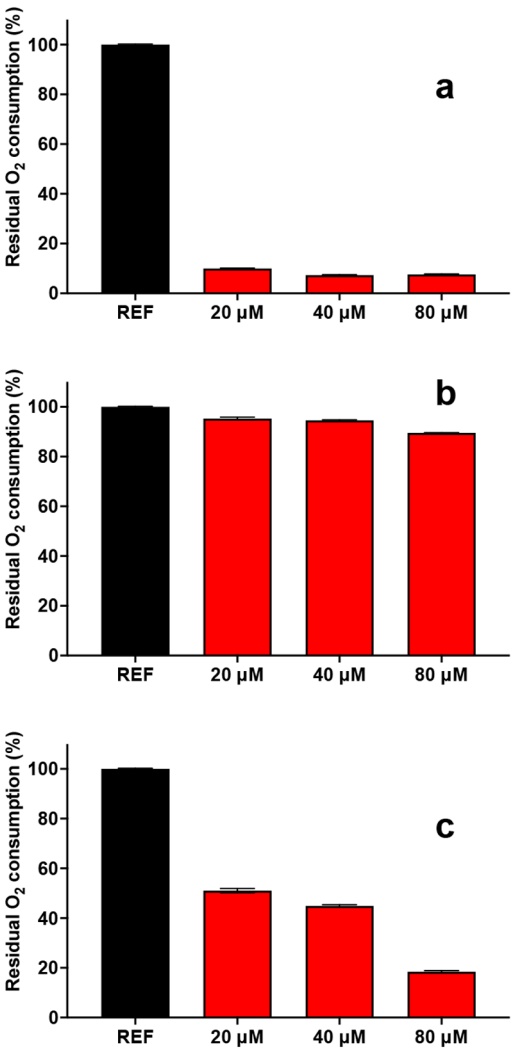

Figure 12. Residual O_2 consumption by *N. europaea* in the presence of increasing concentrations of β-CD·TMTD (a) and $(\beta\text{-CD})_2$·TETD at t = 0 (b), and $(\beta\text{-CD})_2$·TETD at t = 2 h (c).

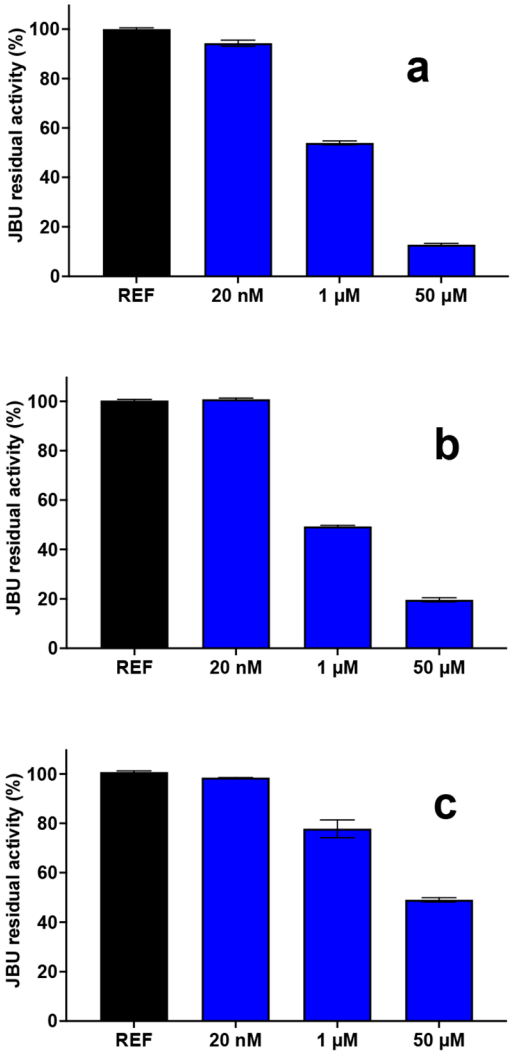

Figure 13. Residual enzymatic activity of JBU in the presence of increasing concentrations of β-CD·TMTD (a), $(\beta\text{-CD})_2$·TETD (b), and $(\beta\text{-CD})_2$·TIPTD (c).

nitrification inhibitor (Figure 12a) with only a minor decrease of inhibition potency as compared to the free compound (compare with Figure 3a). On the other hand, $(\beta\text{-CD})_2$·TETD did not display any significant effect on nitrification (Figure 12b). Considering the limited effect of free TIPTD on nitrification by whole cells of *N. europaea*, the effect of $(\beta\text{-CD})_2$·TIPTD was not investigated. The effect of a 2-h incubation time was monitored for $(\beta\text{-CD})_2$·TETD (Figure 12c) to verify its behavior compared to the free inhibitor (see Figures 3b), again confirming that a much stronger effect on nitrification is obtained if time is allowed for this large adduct to cross the outer bacterial membrane.

The inhibition of urease activity of β-CD·TMTD (Figure 13a), $(\beta\text{-CD})_2$·TETD (Figure 13b), and $(\beta\text{-CD})_2$·TIPTD (Figure 13c) was significant and comparable to that of the free compounds (compare with Figure 3a–c).

The essentially equivalent urease inhibition efficacy of the β-CD adducts and that of the corresponding pure compounds suggests that the active species in this case is the free molecule, which must be in equilibrium with the adduct in solution.

CONCLUSIONS

In this study, we have investigated the capability of three thiurams to modulate the catalytic activity of urease and ammonia monooxygenase. In particular, we have discovered that, among the tested compounds, thiram (tetramethylthiuram disulfide, TMTD) is by far the best inhibitor of both urease and AMO, while disulfiram (tetraethylthiuram disulfide, TETD) and tetraisopropylthiuram disulfide (TIPTD) show a progressively decreasing effect, suggesting the role of steric hindrance of the methyl, ethyl, and isopropyl groups on these compounds. Their utilization as pure compounds, however, is hindered by their extreme insolubility in water. We have demonstrated that their solubility can be significantly improved if the inclusion compounds (β-CD)·TMTD, $(\beta\text{-CD})_2$·TETD, and $(\beta\text{-CD})_2$·TIPTD, prepared using solvent-free mechanochemical methods, are used. These novel compounds were fully characterized by X-ray diffraction, thermogravimetry, and solid-state NMR, obtaining firm evidence for the encapsulation of the active compounds within the cyclodextrin shell. The performance of the inclusion compounds is comparable to that of the pure thiurams, which, if solubility is considered, implies that utilization of these materials as concomitant efficacious

https://doi.org/10.1021/acs.cgd.2c00439
Cryst. Growth Des. 2022, 22, 4528−4537

inhibitors of both nitrification and organic nitrogen mineralization can be envisaged in the framework of sustainable primary production.

■ ASSOCIATED CONTENT

Supporting Information

The Supporting Information is available free of charge at https://pubs.acs.org/doi/10.1021/acs.cgd.2c00439.

Single-crystal and powder X-ray diffraction, Pawley refinement, solid-state NMR spectra, TGA measurements, DSC, solubility data (PDF)

Accession Codes

CCDC 2166004 contains the supplementary crystallographic data for this paper. These data can be obtained free of charge via www.ccdc.cam.ac.uk/data_request/cif, or by emailing data_request@ccdc.cam.ac.uk, or by contacting The Cambridge Crystallographic Data Centre, 12 Union Road, Cambridge CB2 1EZ, UK; fax: +44 1223 336033.

■ AUTHOR INFORMATION

Corresponding Authors

Fabrizia Grepioni − *Department of Chemistry "Giacomo Ciamician", University of Bologna, 40126 Bologna, Italy;* orcid.org/0000-0003-3895-0979; Email: fabrizia.grepioni@unibo.it

Roberto Gobetto − *Department of Chemistry, University of Turin, 10125 Torino, Italy;* orcid.org/0000-0002-2431-8051; Email: roberto.gobetto@unito.it

Stefano Ciurli − *Laboratory of Bioinorganic Chemistry, Department of Pharmacy and Biotechnology, University of Bologna, 40127 Bologna, Italy;* orcid.org/0000-0001-9557-926X; Email: stefano.ciurli@unibo.it

Authors

Lucia Casali − *Department of Chemistry "Giacomo Ciamician", University of Bologna, 40126 Bologna, Italy*

Luca Mazzei − *Laboratory of Bioinorganic Chemistry, Department of Pharmacy and Biotechnology, University of Bologna, 40127 Bologna, Italy;* orcid.org/0000-0003-1335-9365

Renren Sun − *Department of Chemistry "Giacomo Ciamician", University of Bologna, 40126 Bologna, Italy; School of Chemical Engineering, Zhengzhou University, 450001 Zhengzou, Henan Province, The People's Republic of China*

Michele R. Chierotti − *Department of Chemistry, University of Turin, 10125 Torino, Italy;* orcid.org/0000-0002-8734-6009

Dario Braga − *Department of Chemistry "Giacomo Ciamician", University of Bologna, 40126 Bologna, Italy;* orcid.org/0000-0003-4162-4779

Complete contact information is available at: https://pubs.acs.org/10.1021/acs.cgd.2c00439

Author Contributions

#L.C. and L.M. contributed equally to the work.

Notes

The authors declare no competing financial interest.

■ ACKNOWLEDGMENTS

The authors acknowledge financial support from the University of Bologna (F.G., D.B., S.C.), the Consorzio Interuniversitario di Risonanze Magnetiche di Metallo-Proteine (CIRMMP) (S.C., L.M.), and the PRIN 2020 "Nature Inspired Crystal Engineering (NICE)". The China Scholarship Council is acknowledged (R.S.) for a Visiting Ph.D. Student State Scholarship. Dr. Valquiria Broll and Dr. Stefano Alpi are duly acknowledged for carrying out experiments on nitrification inhibition.

■ REFERENCES

(1) Evans, A. *The Feeding of the Nine Billion: Global Food Security*; Chatham House: London, 2009.

(2) Godfray, H. C. J.; Beddington, J. R.; Crute, I. R.; Haddad, L.; Lawrence, D.; Muir, J. F.; Pretty, J.; Robinson, S.; Thomas, S. M.; Toulmin, C. Food security: the challenge of feeding 9 billion people. *Science* **2010**, *327* (5967), 812−818.

(3) Roy, R. N.; Finck, A.; Blair, G. J.; Tandon, H. L. S. *Plant Nutrition for Food Security*; Food and Agriculture Organization of the United Nations: Rome, 2006; p 348.

(4) Beeckman, F.; Motte, H.; Beeckman, T. Nitrification in agricultural soils: impact, actors and mitigation. *Curr. Opin. Biotechnol.* **2018**, *50*, 166−173.

(5) Prud'homme, M. Global fertilizer supply and trade 2016−2017. https://www.fertilizer.org/ItemDetail?iProductCode=10192Pdf&Category=ECO.

(6) Maroney, M. J.; Ciurli, S. Nonredox nickel enzymes. *Chem. Rev.* **2014**, *114* (8), 4206−28.

(7) Mazzei, L.; Musiani, F.; Ciurli, S. Urease. In *The Biological Chemistry of Nickel*; Zamble, D.; Rowińska-Żyrek, M., Kozłowski, H., Eds.; Royal Society of Chemistry, 2017; pp 60−97.

(8) Mazzei, L.; Musiani, F.; Ciurli, S. The structure-based reaction mechanism of urease, a nickel dependent enzyme: tale of a long debate. *J. Biol. Inorg. Chem.* **2020**, *25* (6), 829−845.

(9) Arp, D. J.; Chain, P. S.; Klotz, M. G. The impact of genome analyses on our understanding of ammonia-oxidizing bacteria. *Annu. Rev. Microbiol.* **2007**, *61*, 503−528.

(10) van Kessel, M. A. H. J.; Speth, D. R.; Albertsen, M.; Nielsen, P. H.; Op den Camp, H. J. M.; Kartal, B.; Jetten, M. S. M.; Lücker, S. Complete nitrification by a single microorganism. *Nature* **2015**, *528*, 555.

(11) Musiani, F.; Broll, V.; Evangelisti, E.; Ciurli, S. The model structure of the copper-dependent ammonia monooxygenase. *J. Biol. Inorg. Chem.* **2020**, *25* (7), 995−1007.

(12) Zhang, X.; Davidson, E. A.; Mauzerall, D. L.; Searchinger, T. D.; Dumas, P.; Shen, Y. Managing nitrogen for sustainable development. *Nature* **2015**, *528*, 51.

(13) Zhang, X.; Ward, B. B.; Sigman, D. M. Correction to "Global Nitrogen Cycle: Critical Enzymes, Organisms, and Processes for Nitrogen Budgets and Dynamics". *Chem. Rev.* **2020**, *120* (17), 9834.

(14) Maia, L. B.; Moura, J. J. How biology handles nitrite. *Chem. Rev.* **2014**, *114* (10), 5273−357.

(15) Moura, I.; Maia, L. B.; Pauleta, S. R.; Moura, J. J. G. A Bird's Eye View of Denitrification in Relation to the Nitrogen Cycle. In *Metalloenzymes in Denitrification: Applications and Environmental Impacts*; The Royal Society of Chemistry, 2017; pp 1−10.

(16) Coskun, D.; Britto, D. T.; Shi, W.; Kronzucker, H. J. Nitrogen transformations in modern agriculture and the role of biological nitrification inhibition. *Nat. Plants* **2017**, *3*, 17074.

(17) Paulot, F.; Jacob, D. J. Hidden cost of U.S. agricultural exports: particulate matter from ammonia emissions. *Environ. Sci. Technol.* **2014**, *48* (2), 903−908.

(18) Tilman, D.; Fargione, J.; Wolff, B.; D'Antonio, C.; Dobson, A.; Howarth, R.; Schindler, D.; Schlesinger, W. H.; Simberloff, D.; Swackhamer, D. Forecasting Agriculturally Driven Global Environmental Change. *Science* **2001**, *292* (5515), 281.

(19) Galloway, J. N.; Cowling, E. B. Reactive Nitrogen and The World: 200 Years of Change. *AMBIO* **2002**, *31* (2), 64−71.

(20) Chen, D.; Suter, H.; Islam, A.; Edis, R.; Freney, J. R.; Walker, C. N. Prospects of improving efficiency of fertiliser nitrogen in Australian

agriculture: a review of enhanced efficiency fertilisers. *Aust. J. Soil Res.* **2008**, *46* (4), 289−301.
(21) Timilsena, Y. P.; Adhikari, R.; Casey, P.; Muster, T.; Gill, H.; Adhikari, B. Enhanced efficiency fertilisers: a review of formulation and nutrient release patterns. *J. Sci. Food Agric* **2015**, *95* (6), 1131−42.
(22) Dougherty, W. J.; Collins, D.; Van Zwieten, L.; Rowlings, D. W. Nitrification (DMPP) and urease (NBPT) inhibitors had no effect on pasture yield, nitrous oxide emissions, or nitrate leaching under irrigation in a hot-dry climate. *Soil Res.* **2016**, *54* (5), 675−683.
(23) Friedl, J.; Scheer, C.; Rowlings, D. W.; Deltedesco, E.; Gorfer, M.; De Rosa, D.; Grace, P. R.; Muller, C.; Keiblinger, K. M. Effect of the nitrification inhibitor 3,4-dimethylpyrazole phosphate (DMPP) on N-turnover, the N2O reductase-gene nosZ and N2O:N2 partitioning from agricultural soils. *Sci. Rep.* **2020**, *10* (1), 2399.
(24) Yang, M.; Fang, Y.; Sun, D.; Shi, Y. Efficiency of two nitrification inhibitors (Dicyandiamide and 3, 4-dimethypyrazole phosphate) on soil nitrogen transformations and plant productivity: a meta-analysis. *Sci. Rep.* **2016**, *6*, 22075.
(25) Salis, R. K.; Bruder, A.; Piggott, J. J.; Summerfield, T. C.; Matthaei, C. D. Multiple-stressor effects of Dicyandiamide (DCD) and agricultural stressors on trait-based responses of stream benthic algal communities. *Sci. Total Environ.* **2019**, *693*, 133305.
(26) Moir, J. W.; Crossman, L. C.; Spiro, S.; Richardson, D. J. The purification of ammonia monooxygenase from Paracoccus denitrificans. *FEBS Lett.* **1996**, *387* (1), 71−4.
(27) Burnette, E. M.; Nieto, S. J.; Grodin, E. N.; Meredith, L. R.; Hurley, B.; Miotto, K.; Gillis, A. J.; Ray, L. A. Novel Agents for the Pharmacological Treatment of Alcohol Use Disorder. *Drugs* **2022**, *82* (3), 251−274.
(28) Lu, Y.; Pan, Q.; Gao, W.; Pu, Y.; Luo, K.; He, B.; Gu, Z. Leveraging disulfiram to treat cancer: Mechanisms of action, delivery strategies, and treatment regimens. *Biomaterials* **2022**, *281*, 121335.
(29) Casali, L.; Broll, V.; Ciurli, S.; Emmerling, F.; Braga, D.; Grepioni, F. Facilitating Nitrification Inhibition through Green, Mechanochemical Synthesis of a Novel Nitrapyrin Complex. *Cryst. Growth & Design* **2021**, *21* (10), 5792−5799.
(30) Braga, D. Crystal engineering, Where from? Where to? *Chem. Commun.* **2003**, No. 22, 2751−2754.
(31) Casali, L.; Mazzei, L.; Shemchuk, O.; Sharma, L.; Honer, K.; Grepioni, F.; Ciurli, S.; Braga, D.; Baltrusaitis, J. Novel Dual-Action Plant Fertilizer and Urease Inhibitor: Urea·Catechol Cocrystal. Characterization and Environmental Reactivity. *ACS Sustainable Chem. Eng.* **2019**, *7* (2), 2852−2859.
(32) Gornall, A. G.; Bardawill, C. J.; David, M. M. Determination of serum proteins by means of the biuret reaction. *J. Biol. Chem.* **1949**, *177* (2), 751−766.
(33) Mazzei, L.; Broll, V.; Casali, L.; Silva, M.; Braga, D.; Grepioni, F.; Baltrusaitis, J.; Ciurli, S. Multifunctional Urea Cocrystal with Combined Ureolysis and Nitrification Inhibiting Capabilities for Enhanced Nitrogen Management. *Acs Sustainable Chemistry & Engineering* **2019**, *7* (15), 13369−13378.
(34) Coelho, A. A. *TOPAS-Academic*, V4.1; Coelho Software: Brisbane, Australia, 2007.
(35) Sheldrick, G. M. SHELXT - Integrated Space-Group and Crystal-Structure Determination. *Acta Crystallogr., Sect. A: Found. Adv.* **2015**, *71* (1), 3−8.
(36) Sheldrick, G. M. Crystal Structure Refinement with SHELXL. *Acta Crystallogr., Sect. C: Struct. Chem.* **2015**, *71* (1), 3−8.
(37) Macrae, C. F.; Edgington, P. R.; McCabe, P.; Pidcock, E.; Shields, G. P.; Taylor, R.; Towler, M.; van de Streek, J. Mercury: visualization and analysis of crystal structures. *J. Appl. Crystallogr.* **2006**, *39* (3), 453−457.
(38) Macrae, C. F.; Sovago, I.; Cottrell, S. J.; Galek, P. T. A.; McCabe, P.; Pidcock, E.; Platings, M.; Shields, G. P.; Stevens, J. S.; Towler, M.; Wood, P. A. Mercury 4.0: from visualization to analysis, design and prediction. *J. Appl. Crystallogr.* **2020**, *53* (1), 226−235.
(39) James, S. L.; Adams, C. J.; Bolm, C.; Braga, D.; Collier, P.; Friščić, T.; Grepioni, F.; Harris, K. D. M.; Hyett, G.; Jones, W.; Krebs, A.; Mack, J.; Maini, L.; Orpen, A. G.; Parkin, I. P.; Shearouse, W. C.; Steed, J. W.; Waddell, D. C. Mechanochemistry: opportunities for new and cleaner synthesis. *Chem. Soc. Rev.* **2012**, *41* (1), 413−447.
(40) Caira, M. R. On the isostructurality of cyclodextrin inclusion complexes and its practical utility. *Rev. Roum. Chim.* **2001**, *46*, 371−386.
(41) Azzali, A.; d'Agostino, S.; Grepioni, F. Tuning the Solubility of the Herbicide Bentazon: from Salt to Neutral and to Inclusion Complexes. *ACS Sustainable Chem. Eng.* **2021**, *9* (37), 12530−12539.
(42) Makedonopoulou, S.; Mavridis, I. M.; Yannakopoulou, K.; Papaioannou, J. Organisation of long aliphatic monocarboxylic acids in β-cyclodextrin channels: crystal structures of the inclusion complexes of tridecanoic acid and (Z)-tetradec-7-enoic acid in β-cyclodextrin. *Chem. Commun.* **1998**, 2133−2134.
(43) Félix, O.; Hosseini, M. W.; De Cian, A.; Fischer, J. Crystal engineering of 2-D hydrogen bonded molecular networks based on the self-assembly of anionic and cationic modules. *Chem. Commun.* **2000**, No. 4, 281−282.
(44) Aime, S.; Chierotti, M. R.; Gobetto, R.; Masic, A.; Napolitano, F.; Canuto, H. C.; Heyes, S. J. Intramolecular host-guest dynamics of FeCp(CO)(2)X (X= I and CH3) and Mo2Cp2(CO)(6) included in beta- or gamma-cyclodextrin. *Eur. J. Inorg. Chem.* **2008**, *2008* (1), 152−157.
(45) Jain, P.; He, Y.; Yalkowsky, S. H. *Handbook of Aqueous Solubility Data*, 2nd ed.; CRC Press: 2010.

https://doi.org/10.1021/acs.cgd.2c00439
Cryst. Growth Des. 2022, 22, 4528−4537